Gadolinium Oxide Ultranarrow Nanorods as Multimodal Contrast Agents for Optical and Magnetic Resonance Imaging

ARTICLE *in* LANGMUIR · FEBRUARY 2010

Impact Factor: 4.46 · DOI: 10.1021/la904751q · Source: PubMed

10 AUTHORS, INCLUDING:

Gautom K Das
Rice University
23 PUBLICATIONS **485** CITATIONS
SEE PROFILE

Boon Chin Heng
The University of Hong Kong
232 PUBLICATIONS **3,608** CITATIONS
SEE PROFILE

Tim White
Nanyang Technological University
225 PUBLICATIONS **4,783** CITATIONS
SEE PROFILE

Timothy Thatt Yang Tan
Nanyang Technological University
82 PUBLICATIONS **2,286** CITATIONS
SEE PROFILE

Langmuir
Article
pubs.acs.org/Langmuir

Gadolinium Oxide Ultranarrow Nanorods as Multimodal Contrast Agents for Optical and Magnetic Resonance Imaging

Gautom Kumar Das,[†] Boon Chin Heng,[‡] Sui-Choon Ng,[†] Tim White,[‡] Joachim Say Chye Loo,[‡] Loyola D'Silva,[§] Parasuraman Padmanabhan,[§] Kishore K. Bhakoo,[§] Subramanian Tamil Selvan,*[,⊥] and Timothy Thatt Yang Tan*[,†]

[†]*Division of Chemical and Biomolecular Engineering, School of Chemical and Biomedical Engineering, Nanyang Technological University, 62 Nanyang Drive, Singapore 637459,* [‡]*Division of Materials Science, School of Material Science and Engineering, Nanyang Technological University, Nanyang Avenue, Singapore 637459,* [§]*Translational Molecular Imaging Group, Singapore Bioimaging Consortium, 11 Biopolis Way, Singapore 138667, and* [⊥]*Institute of Materials Research and Engineering, 3 Research Link, Singapore 117602*

Received December 17, 2009. Revised Manuscript Received January 27, 2010

We demonstrate a simple synthetic strategy for the fabrication of single-phase rare earth (RE) doped gadolinium oxide (Gd_2O_3:RE where RE = terbium (Tb), ytterbium (Yb), and erbium (Er)) nanorods (NRs) as multimodal imaging probes. The NRs are ultranarrow and exhibit both emission and magnetic characteristics. The Tb-doped and Yb/Er-codoped Gd_2O_3 NRs exhibit down- and up-conversion fluorescence respectively, and also exhibit paramagnetism. Importantly, these codoped NRs possess excellent magnetic characteristics, as shown in their longitudinal relaxation time (T1) -weighted image contrast, which is closer to that of commercial Gadovist for magnetic resonance imaging (MRI) applications. This property opens up new avenues in the development of contrast agents.

Introduction

In recent years, the development of nanoparticle based contrast agents for multimodal imaging has attracted considerable interest in biomedical research.[1−4] In general, imaging modalities can be broadly categorized into two groups: (I) modalities that provide structural information such as magnetic resonance imaging (MRI), computed tomography (CT), and ultrasound; (II) modalities that provide functional or molecular information such as optical imaging, single photon emission computed tomography (SPECT), and positron emission tomography (PET).[5] Each imaging modality differs from others in detection sensitivity, temporal resolution, spatial resolution, tissue penetration, signal-to-noise and quantitative accuracy. As a consequence, a single imaging modality does not possess complete capabilities to diagnose and understand the fundamental biological process of diseases. However, the combination of modalities can integrate the strengths of individual modality, and at the same time eliminate one or more of their deficiencies.[2,5] Most of the efforts have been devoted toward the fabrication of multimodal imaging contrast agents for multimodal MRI−optical imaging, PET−CT, and PET−optical imaging contrast agents.[6,7]

In particular, significant research attention has been drawn to develop contrast agents for MRI−optical imaging since they ally two useful functionalities: high special resolution of MRI and the high sensitivity of fluorescence imaging. The contrast agents for MRI may produce negative contrast, or positive contrast depending on the agent used. Superparamagnetic iron oxides prevailed among negative contrast agents.[8] Because of the definite structure of superparamagnetic iron oxides, additional features such as luminescence, targeting molecules, and therapeutic agents can be incorporated conveniently to fabricate multifunctional nanostructures for multimodal imaging and therapy.[9−16] In contrast, the development of multimodal nanostructures consisting of the positive contrast agents is limited. Positive contrast agents are mainly metal ions chelates, such as Gd^{3+} (seven unpaired electrons) and Mn^{2+} (five unpaired electrons) chelates.[17] Examples of Gd−chelate based multimodal positive contrast agents include Gd-chealate stabilized-quantum dots,[18] Gd−chelate dendrimer−dye molecules,[19] Gd−chelates conjugated mesoporous silica−dye nanoparticles.[20] However, the metal ion chelates have limitations of being nonspecific to target, quick removal by renal excretion,

*Corresponding authors. (T.T.Y.T) E-mail: tytan@ntu.edu.sg. Telephone: +65 6316 8822. Fax: +65 6794 7553. (S.T.S) E-mail: subramaniant@imre.a-star.edu.sg. Telephone: +65 6874 5249. Fax: +65 6774 4657.

(1) Selvan, S. T.; Tan, T. T. Y.; Yi, D. K.; Jana, N. R. *Langmuir* **2009**, DOI: 10.1021/la903512m.
(2) Cheon, J.; Lee, J.-H. *Acc. Chem. Res.* **2008**, *41*, 1630.
(3) Kim, J.; Piao, Y.; Hyeon, T. *Chem. Soc. Rev.* **2009**, *38*, 372.
(4) Wang, F.; Liu, X. *Chem. Soc. Rev.* **2009**, *38*, 976.
(5) Cherry, S. R. *Annu. Rev. Biomed. Eng.* **2006**, *8*, 35.
(6) Ntziachristos, V.; Yodh, A. G.; Schnall, M.; Chance, B. *Proc. Natl. Acad. Sci. U.S.A.* **2000**, *97*, 2767.
(7) Beyer, T.; Townsend, D. W.; Brun, T.; Kinahan, P. E.; Charron, M.; Roddy, R.; Jerin, J.; Young, J.; Byars, L.; Nutt, R. *J. Nucl. Med.* **2000**, *41*, 1369.
(8) Sun, C.; Lee, J. S. H.; Zhang, M. *Adv. Drug Deliver.Rev.* **2008**, *60*, 1252.
(9) Selvan, S. T.; Patra, P. K.; Ang, C. Y.; Ying, J. Y. *Angew. Chem., Int. Ed.* **2007**, *46*, 2448.
(10) Gao, J.; Zhang, W.; Huang, P.; Zhang, B.; Zhang, X.; Xu, B. *J. Am. Chem. Soc.* **2008**, *130*, 3710.
(11) Lu, H.; Yi, G.; Zhao, S.; Chen, D.; Guo, L.-H.; Cheng, J. *J. Mater. Chem.* **2004**, *14*, 1336.
(12) Kim, H.; Achermann, M.; Balet, L. P.; Hollingsworth, J. A.; Klimov, V. I. *J. Am. Chem. Soc.* **2005**, *127*, 544.
(13) Kircher, M. F.; Mahmood, U.; King, R. S.; Weissleder, R.; Josephson, L. *Cancer Res.* **2003**, *63*, 8122.
(14) Yi, D. K.; Selvan, S. T.; Lee, S. S.; Papaefthymiou, G. C.; Kundaliya, D.; Ying, J. Y. *J. Am. Chem. Soc.* **2005**, *127*, 4990.
(15) Kim, J.; Lee, J. E.; Lee, S. H.; Yu, J. H.; Lee, J. H.; Park, T. G.; Hyeon, T. *Adv. Mater.* **2008**, *20*, 478.
(16) Zhang, Y.; Das, G. K.; Xu, R.; Tan, T. T. Y. *J. Mater. Chem.* **2009**, *19*, 3696.
(17) Bottrill, M.; Kwok, L.; Long, N. J. *Chem. Soc. Rev.* **2006**, *35*, 557.
(18) Mulder, W. J. M.; Koole, R.; Brandwijk, R. J.; Storm, G.; Chin, P. T. K.; Strijkers, G. J.; de Mello Donega, C.; Nicolay, K.; Griffioen, A. W. *Nano Lett.* **2006**, *6*, 1.
(19) Talanov, V. S.; Regino, C. A. S.; Kobayashi, H.; Bernardo, M.; Choyke, P. L.; Brechbiel, M. W. *Nano Lett.* **2006**, *6*, 1459.
(20) Taylor, K. M. L.; Kim, J. S.; Rieter, W. J.; An, H.; Lin, W.; Lin, W. *J. Am. Chem. Soc.* **2008**, *130*, 2154.

and short accumulation time.[21,22] Alternatively, Gd-based inorganic nanoparticles such as gadolinium oxide,[22,23] gadolinium fluorides[24] have been investigated and emerging as potential positive contrast agents. For example, Fortin et al.[23] demonstrated that poly(ethylene glycol) coated ultrasmall Gd_2O_3 (~3 nm) nanoparticles exhibited good relaxivity, about twice as high as Gd−DTPA chelates. Multimodal contrast agents have also been demonstrated using inorganic Gd_2O_3 nanoparticles. For example, Bridot et al.[22] reported multimodal Gd_2O_3 (~4.6 nm) nanoparticles encapsulated within a shell of fluorescent organic fluorophores.

Hence, the abundance of literature have reported the fabrication of multimodal nanostructures, integrating the functionalities by means of: (i) heterodimer formation,[9,10] (ii) core/shell structure formation,[11,12,22] (iii) direct grafting of organic dyes on magnetic nanoparticles,[13] and (iv) encapsulation of magnetic and fluorescent nanoparticles in silica or polymer shells.[14,15] In comparison, the notion of synthesizing single-phase multimodal nanocrystals (NCs) would be favorable in terms of ease of large scale synthesis and functional homogenization.[16,25] On another aspect, tailoring morphology, composition, and surface properties remains a challenge in nanomaterials research. Reported morphologies include the following: 0-dimensional spheres, cubes, and polyhedrons; 1D rods and wires; 2D disks, ribbons, plates; and complex shapes such as tetrapods and stellations.[26]

Herein, we report a simple strategy for synthesizing single-phase bifunctional paramagnetic-fluorescent rare earth (RE) doped Gd_2O_3 ultranarrow NRs (with uniform diameters of 2.5 ± 0.3 nm, and lengths of 18.8 ± 5.7 nm), which could be used as potential contrast agents for bimodal optical and magnetic resonance imaging. It is found that these NRs evolve from quasi-spherical Gd_2O_3 NCs, which are either doped with terbium (Tb) or codoped with ytterbium (Yb) and erbium (Er). The uniform-diameter NRs demonstrate both down- and up-conversion fluorescence, are paramagnetic, and also display a good contrast in T1-weighted MRI. From a technological perspective, REs are extremely promising for applications ranging from optoelectronics to fiber amplifiers, solid-state lasers, and biological labels.[25,27,28] RE ions have superior photostability, multicolor emission, and most importantly, have lower toxicity compared to common organic dyes and semiconductor QD probes.[29,30]

Gd_2O_3 was chosen because it constitutes a good host matrix for luminescent RE ions.[31,32] In addition, it shows paramagnetic properties[22,23,33] which make Gd_2O_3 a very attractive choice to dope with different RE ions for achieving single-phase bifunctionality (i.e., paramagnetism and multicolor emission). Contrast agents derived from ultrasmall nanotubes (NTs)/nanorods have been reported to be highly promising for intracellular imaging.[34,35] NTs/NRs of size range of 20−100 nm are believed to be best suited for cellular uptake, biocompatibility and eventual elimination from the body.[36] The synthesis of NTs or NRs as potential bioimaging probes have been mostly demonstrated on II−VI semiconductor quantum dots (QDs) that are luminescent from the mid-infrared to visible,[37,38]and modified single walled carbon nanotubes (SWNT).[35,36,39] Gd^{3+}-ion loaded SWNTs for MRI have also been reported.[36] However, to the best of our knowledge, there is no report of single-phase bifunctional gadolinium oxide (Gd_2O_3) ultranarrow NRs which could potentially be used as contrast agents for bimodal optical/MR imaging. Thus, our main endeavor is to report the potential of single-phase Gd_2O_3 ultranarrow NRs as bimodal contrast agent.

Experimental Section

Materials. All chemicals were used as received without further purifications. Gadolinium(III) oxide (99.99%), terbium(III) chloride hexahydrate (99.9%), ytterbium(III) chloride hexahydrate (99.99%), erbium(III) chloride hexahydrate (99.9%), tetramethylammonium hydroxide (25 wt % in methanol) (TMAH) Igepal CO-520 (Polyoxyethylene(5)nonylphenyl ether), and oleylamine (tech., 70%), were purchased from Aldrich. HNO_3 (analytical reagent, 70%), and oleic acid (tech. 90%) were purchased from Alfa Aesar. NaOH (reagent grade, 97%, beads) and 3-aminopropyltrimethoxysilane (APS) (97%) were purchased from Fluka. Ethanol, hexane, cyclohexane, and chloroform were of analytical reagent grade.

Synthesis of RE-Doped Gd_2O_3 NCs and NRs. Typically, 2 mmol (0.725 g) of Gd_2O_3 and 0.22 mmol (0.082 g) of $TbCl_3.6H_2O$ were dissolved in 0.8 mL HNO_3 (70%). To this acidic solution, 6 mL of H_2O, 9 mL of ethanol, 15 mL of hexane and 2−4 mL of oleic acid were added in sequence and the mixture stirred in a closed vessel at 70 °C for 2 h. A second solution, prepared by dissolving 0.24 g of NaOH in 6 mL of H_2O was then added dropwise and heated at 70 °C with stirring for another 4 h. After reaction, the mixture separated into two transparent layers. The upper organic layer containing the Gd−Tb−oleate complex was collected, washed with 30 mL of distilled water and dried overnight in an oven at 70 °C to evaporate water and hexane. The waxy Gd−Tb−oleate complex obtained after drying was dissolved in 20 mL of oleylamine in a three-neck flask and purged with N_2. The solution was then heated to 300 °C at a rate of 5 °C/min under the blanket of N_2. First NCs emerged and then NRs were grown in the solution at different reflux times. The mixture was cooled to room temperature before precipitation and purified by centrifugation with extensive ethanol washing. The NRs were finally dispersed in cyclohexane for further characterization. For Yb/Er-codoped samples, 0.36 mmol (0.138 g) of $YbCl_3 \cdot 6H_2O$ and 0.12 mmol (0.045 g) $ErCl_3 \cdot 6H_2O$ were used, instead of $TbCl_3 \cdot 6H_2O$.

Silanization of the RE-Doped Gd_2O_3 NRs and NCs. Silanization of the NRs was performed according to the method

(21) Morawski, A. M.; Lanza, G. A.; Wickline, S. A. *Curr. Opin. Biotech.* **2005**, *16*, 89.
(22) Bridot, J.-L.; Faure, A.-C.; Laurent, S.; Riviere, C.; Billotey, C.; Hiba, B.; Janier, M.; Josserand, V.; Coll, J.-L.; Vander Elst, L.; Muller, R.; Roux, S.; Perriat, P.; Tillement, O. *J. Am. Chem. Soc.* **2007**, *129*, 5076.
(23) Fortin, M.-A.; R. M. P., Jr.; Söderlind, F.; Klasson, A.; Engström, M.; Veres, T.; Käll, P.-O.; Uvdal, K. *Nanotechnology* **2007**, *18*, 395501.
(24) Evanics, F.; Diamente, P. R.; van Veggel, F. C. J. M.; Stanisz, G. J.; Prosser, R. S. *Chem. Mater.* **2006**, *18*, 2499.
(25) Shen, J.; Sun, L.-D.; Yan, C.-H. *Dalton Trans.* **2008**, *42*, 5687.
(26) Young-wook, J.; Jin-sil, C.; Jinwoo, C. *Angew. Chem., Int. Ed.* **2006**, *45*, 3414.
(27) Kenyon, A. J. *Prog. Quant. Electron.* **2002**, *26*, 225.
(28) Boyer, J.-C.; Manseau, M.-P.; Murray, J. I.; van Veggel, F. C. J. M. *Langmuir* **2009**, DOI: 10.1021/la902260j.
(29) Goldys, E. M.; Drozdowicz-Tomsia, K.; Jinjun, S.; Dosev, D.; Kennedy, I. M.; Yatsunenko, S.; Godlewski, M. *J. Am. Chem. Soc.* **2006**, *128*, 14498.
(30) Das, G. K.; Chan, P. P. Y.; Teo, A.; Loo, J. S. C.; Anderson, J. M.; Tan, T. T. Y. *J. Biomed. Mater. Res. A* **2009**, DOI: 10.1002/jbm.a.32533.
(31) Louis, C.; Bazzi, R.; Marquette, C. A.; Bridot, J.-L.; Roux, S.; Ledoux, G.; Mercier, B.; Blum, L.; Perriat, P.; Tillement, O. *Chem. Mater.* **2005**, *17*, 1673.
(32) Guo, H.; Dong, N.; Yin, M.; Zhang, W.; Lou, L.; Xia, S. *J. Phys. Chem. B* **2004**, *108*, 19205.
(33) Huang, C.-C.; Liu, T.-Y.; Su, C.-H.; Lo, Y.-W.; Chen, J.-H.; Yeh, C.-S. *Chem. Mater.* **2008**, *20*, 3840.
(34) Lu, Q.; Moore, J. M.; Huang, G.; Mount, A. S.; Rao, A. M.; Larcom, L. L.; Ke, P. C. *Nano Lett.* **2004**, *4*, 2473.
(35) Shi Kam, N. W.; Jessop, T. C.; Wender, P. A.; Dai, H. *J. Am. Chem. Soc.* **2004**, *126*, 6850.
(36) Sitharaman, B.; Kissell, K. R.; Hartman, K. B.; Tran, L. A.; Baikalov, A.; Rusakova, I.; Sun, Y.; Khant, H. A.; Ludtke, S. J.; Chiu, W.; Laus, S.; Toth, E.; Helm, L.; Merbach, A. E.; Wilson, L. *Chem. Commum.* **2005**, 3915.
(37) Acharya, S.; Gautam, U. K.; Sasaki, T.; Bando, Y.; Golan, Y.; Ariga, K. *J. Am. Chem. Soc.* **2008**, *130*, 4594.
(38) Chin, P. T. K.; Stouwdam, J. W.; Janssen, R. A. J. *Nano Lett.* **2009**, *9*, 745.
(39) Miyawaki, J.; Matsumura, S.; Yuge, R.; Murakami, T.; Sato, S.; Tomida, A.; Tsuruo, T.; Ichihashi, T.; Fujinami, T.; Irie, H.; Tsuchida, K.; Iijima, S.; Shiba, K.; Yudasaka, M. *ACS Nano* **2009**, *3*, 1399.

described by Selvan et al.[9] At first, reverse micelles were prepared by dissolving 0.2 g of Igepal CO-520 in 4 mL of cyclohexane, followed by vigorous stirring for 30 min. Meanwhile, NRs were redispersed in chloroform at a concentration of 4 mg/mL and added 1 mL to the micelle solution and stirred for 15 min. Subsequently, 30 μL of APS was added and the mixture was stirred for another 1 h. Then, 30 μL of TMAH in methanol was added. After additional 1 h of stirring, 20 μL of deionized water was added and stirred for 30 min. At this stage, globules of silanized NRs were formed and settled at the bottom of the flask, leaving the upper solution transparent. The globules were then collected and the transparent organic phase was discarded. After this, the NRs were washed with chloroform and ethanol for the complete removal of excess surfactant and other reactants and finally dispersed in deionized water. Silanization of the NCs was performed using the same process but with 25 μL of APS, 25 μL TMAH, and 15 μL of deionized water. The NRs were then used in T1-weighted MR imaging and both NCs and NRs were used in cytotoxicity studies.

Characterization of Nanoparticles. *Transmission Electron Microscopy*. The high resolution transmission electron microscopy (HRTEM), transmission electron microscopy (TEM), and selected area electron diffraction (SAED) were acquired using a JEOL JEM-2100F microscope operating at 200 kV. A drop of nanoparticle dispersion was put onto a holey carbon film supported on a 200 mesh copper grid (3 mm in diameter) and allowed to dry in air at room temperature. The carbon grid with sample was then mounted into the vacuum chamber for imaging and SAED.

Powder X-ray Diffraction. Approximately, 40−50 mg of a sample was stirred gently in an agate mortar to break up lumps. The powdery samples of the nanoparticles were then spread evenly onto a zero-background holder. Step-scan X-ray powder diffraction data were collected over the range of 2θ range of 10−85° on a D8 Advance Bruker powder X-ray diffractometer with Cu Kα (operated at 40 kV, 40 kA) radiation (λ = 0.15406 nm) with 6 mm divergence slit, 1 mm scattering slit, and 0.2 mm receiving slit. The scanning step size was 0.015° in 2θ with a counting time of 1 s per step.

Energy Dispersive X-ray Spectroscopy. Energy-dispersive X-ray (EDX) spectroscopy was done using a high resolution transmission electron microscope (JEOL, JEM 2100-F, Japan) operating at 200 kV and EDS (EDAX, AMETEK, USA, system resolution: 135 eV). Few drops of nanoparticle dispersion were put onto a holey carbon film supported on a 200 mesh copper grid (3 mm in diameter) and allowed to dry in air at room temperature. The carbon grid with sample was then mounted into the vacuum chamber for elemental compositional analysis.

Fluorescence Studies. Nanoparticle samples were dispersed in cyclohexane in a standard suare quartz cuvette at room temperature and their fluorescence properties were studied. Up-conversion fluorescence spectra were obtained using a Fluoromax-4, Horiba Jobin Yvon Spectrofluorometer, which employs a photon-counting detection system for detecting fluorescence emission. To obtain the emission spectra, sample excitation was accomplished using a diode laser, BWF-2 (980 nm, P_{max} = 2.0 W at 3.0 A, B&W TEK Inc.) coupled to a 100 μm (core) optical fiber. The emission spectra in the visible region was obtained with a resolution of 1 nm and a laser power of 0.75 W. Down-conversion fluorescence spectra were obtained using a Shimadzu RF-5301 PC Spectrofluorometer fitted with a 150 W xenon lamp as the excitation source with a resolution of 1 nm.

Vibrating Sample Magnetometer (*VSM*). The magnetization values of the samples were acquired at room temperature with a LakeShore 7400 vibrating sample magnetometer (VSM) instrument using an applied magnetic field from 0 to 1 T. Approximately 10 mg dry powder samples were used for magnetization measurements.

Magnetic Resonance Imaging (*MRI*). The T1-weighted images were obtained on a Varian 9.4T MRI system. All samples were dissolved in double distilled water. The repetition time (TR) and echo time (TE) values were optimized for T1-weighting while using the spin echo sequence. Other parameters used for imaging are: number of acquisitions = 25, field of view = 35 mm, slice thickness = 3 mm, and acquisition time ~ 6 min/sample. All experiments were performed in 1% agarose medium.

Cytotoxicity Studies of Tb-Doped NRs and NCs. Human bronchial epithelial cells (BEAS-2B) were seeded on 12-well culture plates (~4.8 cm^2 per well) at a density of 1.0×10^4 cells/cm^2. The culture media was composed of Dulbecco's Minimum Essential Medium (DMEM) supplemented with 10% (v/v) fetal bovine serum (FBS) and 1% (v/v) antibiotic-antimycotic solution (Sigma-Aldrich Inc.). The seeded cells were cultured for 24 h prior to the loading of nanoparticles. Gd_2O_3:Tb NCs and NRs was chosen for the cell viability experiments.

The following day after seeding, the BEAS-2B cells were exposed to varying concentrations (0, 100, and 250 μg/mL) of Gd_2O_3:Tb NRs and NCs constituted in culture media (1 mL per well) for 72 h at 37 °C within a 5% CO_2 incubator. Prior to incubation with the BEAS-2B cells, the Gd_2O_3:Tb NRs and NCs constituted in culture media were sonicated for 15 min with an ultrasonic cleaner (MRC laboratory instruments Inc., Holon, Israel). Altogether, there were three replicates for each Gd_2O_3:Tb nanoparticle concentration, and also for the negative control. Subsequently after 72 h of culture, the cells were subjected to the WST-8 assay[40] to quantify the proportion of cells that remained viable after exposure to varying concentrations of Gd_2O_3:Tb NRs and NCs. The CCK-8 kit (Dojindo Molecular Laboratories Inc., Kumamoto, Japan) were used for cell counting which utilizes the water-soluble tetrazolium salt WST-8 (2-(2-methoxy-4-nitrophenyl)-3-(4-nitrophenyl)-5-(2,4-disulfophenyl)-2*H*-tetrazolium,monosodium salt) in measuring NADH production resulting from the dehydrogenase activity of viable cells. The subsequent reduction of WST-8 by viable cells produces an orange-colored formazan product with an absorbance at 450 nm. The cells were washed three times in PBS (phosphate buffered saline), prior to the addition of 25 μL of CCK-8 solution and 225 μL of culture media within each well of the 12-well culture plate. After incubation for 2 h at 37 °C within a 5% CO_2 incubator, 100 μL aliquot of the reaction mixture were transferred into a fresh 96-well plate, and absorbance was measured at 450 nm using an Infinite200 microplate reader (Tecan Inc., Maennedorf, Switzerland). The cell viability upon exposure to different concentrations of Gd_2O_3:Tb NRs and NCs, was calculated as the ratio of absorbance readings (450 nm) yielded by the treated and untreated (negative control) wells, after correction of blank absorbance of the reaction mixture incubated without cells for the same duration at 37 °C.

Results and Discussion

The controlled decomposition of RE-doped Gd-oleate complex at a fixed reaction temperature of 300 °C resulted in compositionally independent morphological evolution. The TEM images of Tb-doped and Yb/Er-codoped Gd_2O_3 NCs and NRs are broadly similar; hence the images of Tb-doped Gd_2O_3 are presented as representative ones. Typically, monodisperse quasi-spherical Gd_2O_3:RE (RE = Tb, Yb/Er) NCs of 2.5 ± 0.3 nm in diameter (measured over 70 NCs) are produced after refluxing for 10 min (Figure 1a). The crossed lattice is clearly visible for a NC (upper inset of Figure 1a) and the interplanar distance was measured to be 0.31 nm, which corresponds to the (222) planes of cubic Gd_2O_3. The X-ray diffraction (XRD) pattern (Figure 2a) is consistent with the body-centered cubic

(40) Ishiyama, M.; Miyazono, Y.; Sasamoto, K.; Ohkura, Y.; Ueno, K. *Talanta* **1997**, *44*, 1299.

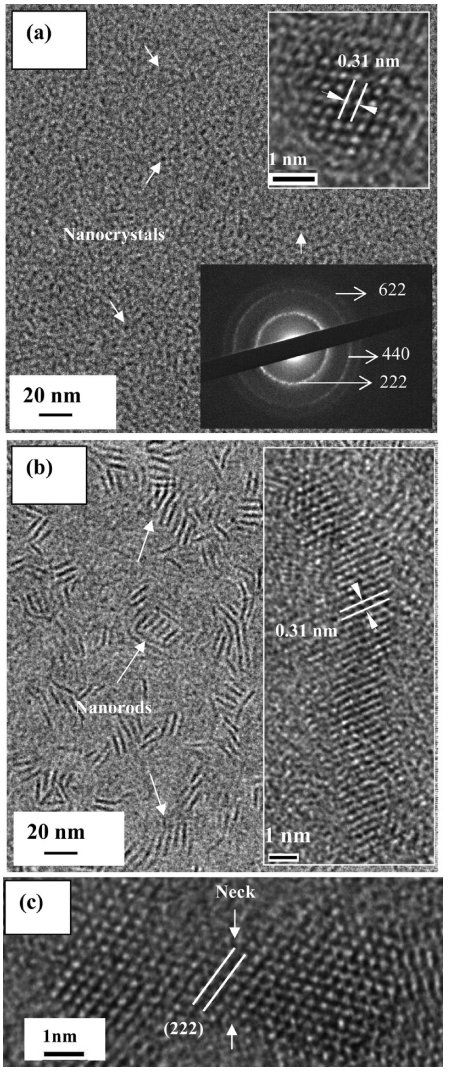

Figure 1. (a) TEM image of monodisperse Gd_2O_3:Tb NCs; Upper inset: HRTEM of a single NC; Lower inset: Selected area electron diffraction (SAED) pattern of Gd_2O_3:Tb NRs. (b) TEM image of monodisperse Gd_2O_3:Tb NRs. Inset: HRTEM image of a single NR showing interplanar distance equivalent to (222) planes. (c) HRTEM image of a dimer fused together, creating a neck.

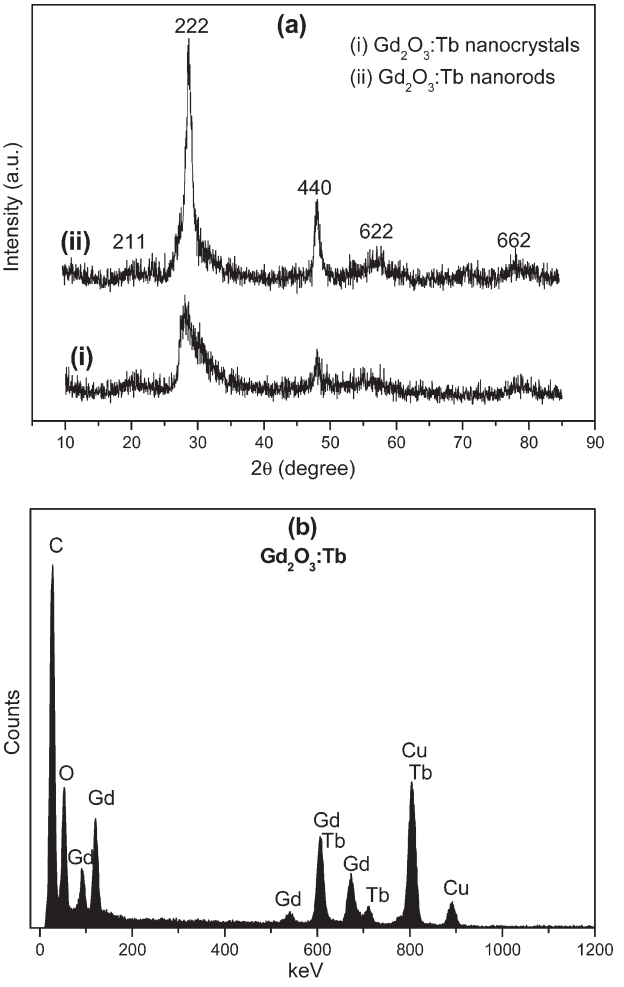

Figure 2. (a) Typical XRD patterns of (i) Gd_2O_3:Tb NCs and (ii) NRs. (b) Energy dispersive X-ray (EDX) analysis of Gd_2O_3: Tb NRs.

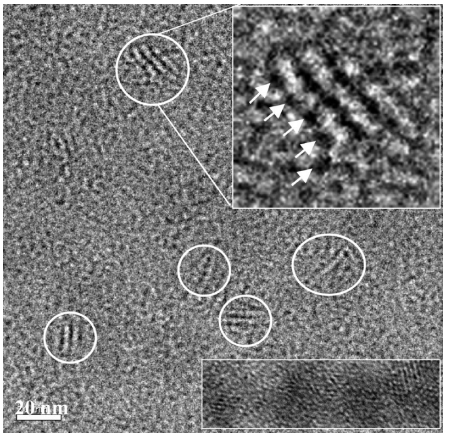

Figure 3. TEM images of samples at early stage of growth showing the formation of pearl necklace-like chains. The marked circles show regions where chains of NCs are observed. Upper inset: The magnified portion of the indicated region. Each arrow indicates individual nanocrystal forming into chain. Lower inset: Fusion of NCs.

structure of gadolinium oxide (JCPDS File No. 00−011−0604). However, it is noted that the symmetry is probably pseudocubic as the peak shape of the (222) reflection is anisotropic. The wide diffraction peaks are consistent with nanocrystallite size, with Scherrer line-width analysis yielding a particle diameter of 2.6 nm, in agreement with TEM. As refluxing progresses, NCs evolve into NRs and after 30 min, a few nanosized oligomers and NRs are observed (Figure S1a (Supporting Information)). After 1 h, most of the NCs are fused into NRs (Figure S1b) and after 2 h the evolution is essentially complete (Figure 1b). The diameters of the NRs remained similar as NCs while lengths were measured to be 18.8 ± 5.7 nm. The TEM image of a large population of NRs at low magnification and also their size distribution (measured over 80 NRs) are shown in Figure S2 (Supporting Information). The Gd_2O_3:Tb NRs display preferred growth on (222) planes (right inset of Figure 1b) that matches well with XRD (Figure 2a(ii)), where the (222) reflection is enhanced compared to the NCs. Selected area electron diffraction (SAED) from NRs agglomerates (lower inset of Figure 1a) can be indexed as cubic Gd_2O_3 with (222), (440) and (622) diffraction rings at real space interplanar distances of 0.31, 0.19, and 0.16 nm, respectively. The strongest intensity of (222) diffraction ring may provide further evidence of a preferred orientation to that direction as well. Energy dispersive X-ray (EDX) spectroscopy for Tb-doped Gd_2O_3 is shown in

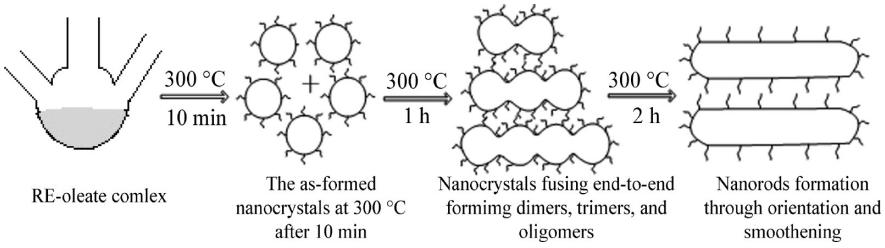

Figure 4. Proposed mechanism of the nanorods formation by oriented attachment.

Figure 2b. The analysis suggests that the concentration of Tb in Gd_2O_3:Tb, is 10.1 mol %, while the EDX spectrum for Yb/Er-codoped Gd_2O_3 suggests that the concentration of Yb and Er in NRs are 14.6 and 3.8 mol %, respectively (Figure S3 (Supporting Information)). The C and Cu peaks are resulted from the capping ligands, oleic acid/oleylamine and copper grid used for TEM, respectively.

The coalescence of two individual Gd_2O_3:Tb NCs by fusion and crystallographical orientation is depicted in Figure 1c, where oriented attachment takes place on (222) planes. This topotaxial creates a neck with fusion along the ⟨111⟩ axis. When many NCs fuse in this fashion, necklace-like chains are created (Figure 3). The formation of pearl necklace-like chains of diameter equal to that of a single NC supports the mechanism of oriented attachment.[38] The latter mechanism has been observed for many different materials forming one-dimensional nanostructures.[38,41−44] The difference in crystal surface energy or dipolar interaction has been proposed as the main driving force for 1D growth. For the cubic Gd_2O_3:RE NCs, we believe that the former (i.e., difference in surface energy) is the most probable cause of chain assembly. During the thermolysis of the precursor complex, capping ligand (type, concentration, and selective adsorption onto crystallographic surface) plays a critical role in morphology control. Our experiment suggested that the ligand—oleylamine has more influence than oleic acid in shape control. Furthermore, oleylamine provides a steric stabilization, thereby preventing the aggregation of particles. The oleylamine adsorbed on the NC surface, changes the surface energies of the crystal facets and growth kinetics, leading to anisotropic structures.[43] The influence of other ligands such as hexadecylamine (HDA), and dodecylamine (DDA) was examined, but they did not promote the formation of uniform NRs as shown in Figure S4 (Supporting Information). The effect of oleic acid was also investigated by varying its volume from 2 to 4 mL in the presence of oleylamine during the Gd−RE−oleate complex preparation step. Only uniform NRs were observed. On the basis of these observations, a simple scheme is devised to elucidate the growth mechanism of the NRs, as shown in Figure 4. First, the NCs form extended chains due to interactions of oleyamine. Second, the chains fuse longitudinally and recrystallize into single crystal ultranarrow NRs. The fusion of NCs eliminates curved spheroid surfaces, which is an enthalpy favorable process.[45] Third, filling of the necks takes place by conventional dissolution and growth of monomers.[42]

The room temperature photoluminescence (PL) spectra of the Tb-doped Gd_2O_3 NRs excited at 235 nm shows down-conversion

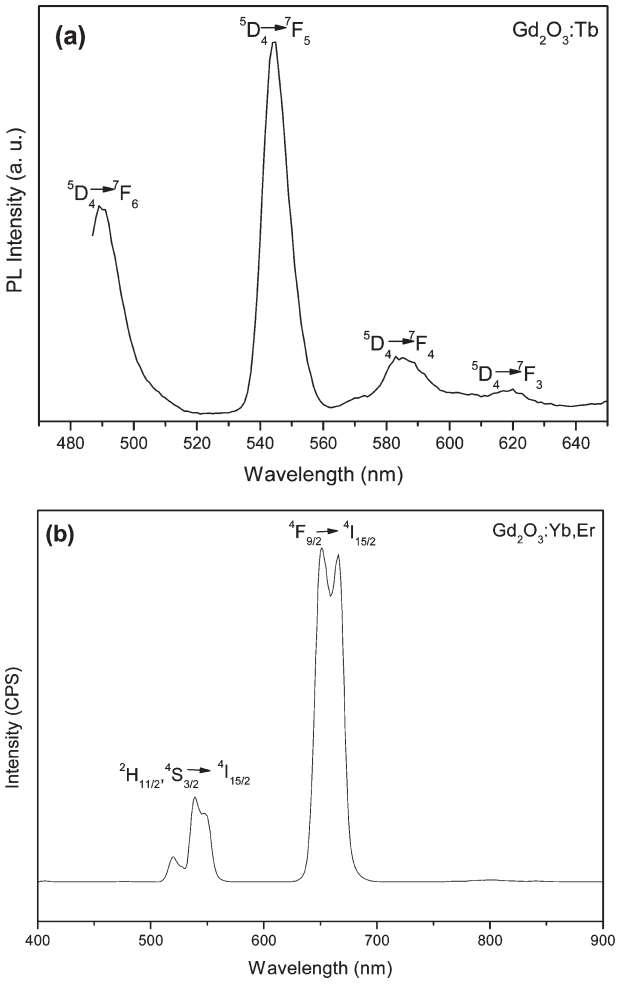

Figure 5. Room temperature (a) down-conversion luminescence spectrum of Tb-doped Gd_2O_3, and (b) up-conversion luminescence spectrum of Yb/Er-codoped Gd_2O_3.

emission (Figure 5a). The characteristic emission peaks of Tb ions appear at 489, 545, 585, and 619 nm from $^5D_4 \rightarrow {}^7F_j$ (j = 6, 5, 4, 3) transitions respectively;[46] the strongest green emission at 545 nm corresponds to the $^5D_4 \rightarrow {}^7F_5$ transition. To demonstrate the versatility of RE ion doping approach for up-conversion emission, we codoped the NRs with Yb and Er ions. The up-conversion luminescence of Yb/Er-codoped Gd_2O_3 NRs at 980 nm excitation is shown in Figure 5b. The up-conversion spectrum shows characteristic Er^{3+} green emissions at 520 and 539 nm, which can be assigned to $^2H_{11/2} \rightarrow {}^4I_{15/2}$ and $^4S_{3/2} \rightarrow {}^4I_{15/2}$ transitions, respectively. The dominant red emission appears

(41) Penn, R. L.; Banfield, J. F. *Geochim. Cosmochim. Acta* **1999**, *63*, 1549.
(42) Pacholski, C.; Weller, A. K. H. *Angew. Chem., Int. Ed.* **2002**, *41*, 1188.
(43) Sigman, M. B.; Ghezelbash, A.; Hanrath, T.; Saunders, A. E.; Lee, F.; Korgel, B. A. *J. Am. Chem. Soc.* **2003**, *125*, 16050.
(44) Cho, K.-S.; Talapin, D. V.; Gaschler, W.; Murray, C. B. *J. Am. Chem. Soc.* **2005**, *127*, 7140.
(45) Penn, R. L.; Banfield, J. F. *Science* **1998**, *281*, 969.
(46) Goldburt, E. T.; Kulkarni, B.; Bhargava, R. N.; Taylor, J.; Libera, M. *J. Lumin.* **1997**, *72−74*, 190.

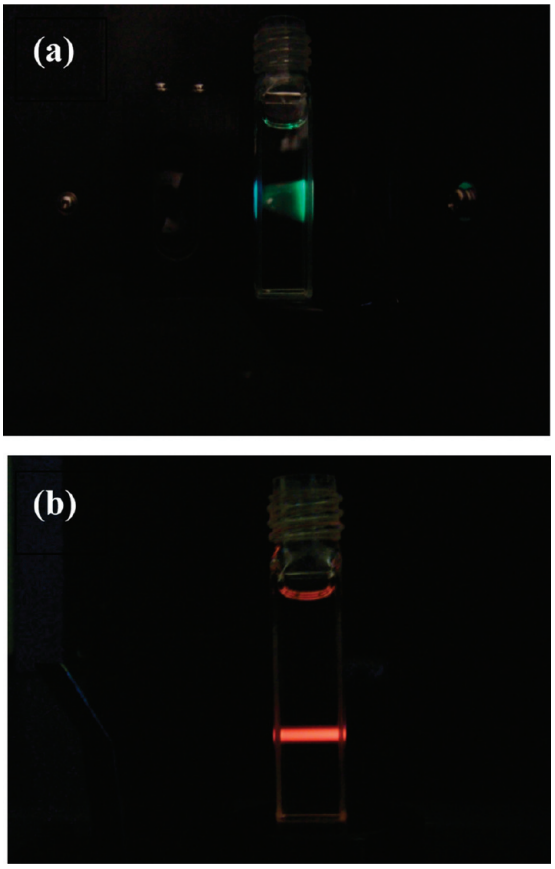

Figure 6. Digital photographs of (a) down-conversion Tb-doped Gd_2O_3 solution exhibiting green emission at 235 nm excitation and (b) up-conversion Yb/Er-codoped Gd_2O_3 solution exhibiting red emission at 980 nm excitation.

between 651 and 667 nm is due to $^4F_{9/2} \rightarrow {}^4I_{15/2}$ transitions.[47,48] Figure 6a shows a digital photograph of a solution of Tb-doped Gd_2O_3 NRs emitting green at 235 nm excitation, which is due to its dominant green emission (at 545 nm). Figure 6b shows a photograph of the up-conversion luminescence of the NRs which appears red due to dominant red emission. The emission intensities from cubic Gd_2O_3 are not very strong and may be optimized by varying dopant concentrations or via surface passivation. Fluoride materials are better hosts for efficient emission. We are currently investigating bifunctional magnetic and up-converting fluoride hosts as potential bimodal imaging probes.

The room temperature magnetization (M) of Gd_2O_3:RE (RE = Tb, Yb/Er), as a function of applied field (H) (−10 to +10 kOe) shows a linear correlation with a magnetization value of 2.46 emu/g (at 10 kOe), suggesting that the Gd_2O_3:RE NRs are paramagnetic (Figure 7a). As a comparison, the room temperature magnetization value reported by Huang et al.[33] is ∼1.25 emu/g (at 10 kOe) for 200 nm porous Gd_2O_3, whereas magnetization of 0.75 emu/g (at 15 kOe) for poly(ethylene glycol)-covered 3 nm Gd_2O_3 is reported by Fortin et al.[23]

To examine the potential application of NRs as MRI contrast agents, the longitudinal relaxation time (T1) -weighted images were acquired for upconversion Gd_2O_3:Yb,Er NRs. As shown in Figure 7b, the T1-weighted MR images of Gd_2O_3:Yb,Er NRs show signal enhancement with increasing Gd^{3+} concentration.

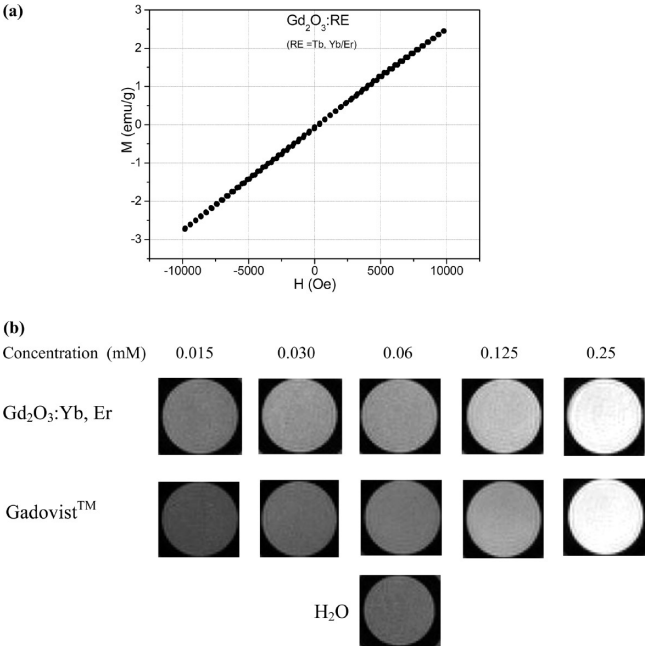

Figure 7. (a) Room temperature magnetization of Gd_2O_3:RE (RE = Tb, Yb/Er). (b) T1-weighted images of Gd_2O_3:Yb,Er and Gadovist at various Gd^{3+}concentrations. T1-weighted image of water sample is shown as reference.

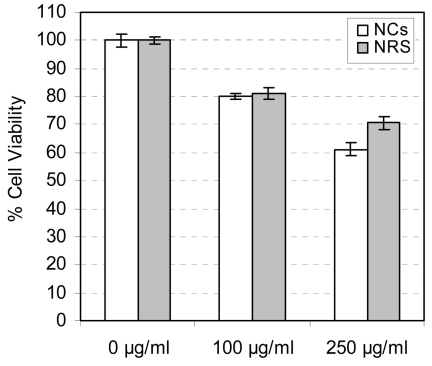

Figure 8. In vitro cell viability of BEAS-2B cells in presence of Gd_2O_3:Tb NCs and NRs at specified concentrations upon exposure for 72 h. The cell viability was estimated using WST-8 assay in triplicate. The error bars indicate mean square standard deviations.

In addition, the T1 and the specific relaxivity (change in relaxation rate per unit concentration, r1) of NRs were determined to be 665 ms and 1.5 $s^{-1}mM^{-1}$, respectively (Figure S5a (Supporting Information)). These values were compared with Gadovist, a commercial Gd-based contrast agent. The observed T1-weighted images (Figure 7b) for Gadovist at different Gd^{3+} concentration reveal that the image contrast of the NRs closely mimics the contrast of Gadovist. The T1 and r1 of Gadovist obtained are 230 ms and 4.34 s^{-1} mM^{-1}, respectively (Figure S3b (Supporting Information)). These results suggest that the NRs are good T1 contrast agents.

In general, free Gd^{3+} ions are cytotoxic and hence are usually ligand-chelated to reduce their toxicity.[49] Therefore, it is necessary to investigate the cytotoxic effect of Gd_2O_3:RE NCs and NRs. For this reason, Gd_2O_3:Tb NCs and NRs were exposed to human bronchial epithelial cells (BEAS-2B) for cell viability study.

(47) Yi, G.; Sun, B.; Yang, F.; Chen, D.; Zhou, Y.; Cheng, J. *Chem. Mater.* **2002**, *14*, 2910.
(48) Boyer, J. C.; Johnson, N. J. J.; van Veggel, F. C. J. M. *Chem. Mater.* **2009**, *21*, 2010.
(49) Li, W.-h.; Fraser, S. E.; Meade, T. J. *J. Am. Chem. Soc.* **1999**, *121*, 1413.

The maximum particle concentration of 250 μg/mL and exposure time of 72 h have been used. The concentration used was slightly higher than the concentration used by Huang et al.[33] in a similar study for evaluating cytotoxicity of hollow and porous Gd_2O_3 nanoparticles. Figure 8 shows the results of the cell viability at different nanoparticle concentrations. At a concentration of 100 μg/mL, the cell viability of NRs was 81.1 $\pm$ 2.0%, which was similar to the cell viability obtained for NCs (79.9 $\pm$ 1.0%). But at a concentration of 250 μg/mL, the cell viability of the NCs (61.0 $\pm$ 2.3%) was lower than that of the NRs (70.6 $\pm$ 2.4%). The observed low cell viability (i.e., $\sim$ 70−80%) are of similar values reported for other type of RE nanoparticles such as $NaYF_4$:Yb, Er[50] and Y_2O_3:Er[30] for different cell lines. Dose-dependent cell viability has been observed for many nanoparticles.[30,33,51] At higher nanoparticle-doses, cells may expose to higher number of toxic ions which lead to low cell viability.[51] But interestingly, we observed lower cell viability for NCs compared to NRs at a higher concentration. The dimensions of NRs are $\sim$2.5 nm $\times$ $\sim$18 nm, as compared to the NCs that has a dimension of $\sim$2.5 nm $\times$ $\sim$2.5 nm. Therefore, for any given mass or concentration, we would expect that there could be six to seven times more NCs compared to NRs that can potentially interact with the cell membrane and be internalized within the cell. It is possible that at higher concentrations, a greater number of NCs results in higher cytoxicity for the cells. However, a comprehensive cytotoxicity study, including a range of cell lines at different exposure conditions and various types of cell viability assays, should be undertaken to elucidate the complete toxic effects of these nanoparticles.

(50) Abdul Jalil, R.; Zhang, Y. *Biomaterials* **2008**, *29*, 4122.
(51) Yin, H.; Too, H. P.; Chow, G. M. *Biomaterials* **2005**, *26*, 5818.

Conclusions

In summary, a facile synthetic strategy has been developed to produce bifunctional RE-doped Gd_2O_3 NRs with tunable optical (down- or up-conversion fluorescence), and magnetic (paramagnetism) properties. More importantly, the Yb/Er-codoped Gd_2O_3 NRs exhibit good T1-weighted MRI contrast, comparable to the commercial product. The simplicity of the methodology to fabricate single-phase magnetic-luminescent Gd_2O_3:RE NCs could potentially lead to a range of bifunctional nanorod architectures and contrast agents in integrated imaging technologies, whereby MRI and florescence microscopy can be combined to provide higher spatial resolution and sensitivity in tissue and cellular imaging.

Acknowledgment. G.K.D. gratefully acknowledges a research scholarship from Nanyang Technological University. The authors thank Ms. Guo Jun at the School of Materials Science and Engineering for her assistance with HRTEM.

Supporting Information Available: Figures S1−S5 showing Gd_2O_3:Tb samples after 30 min of reflux, TEM image of Gd_2O_3:Tb NRs after 2 h of reflux, an energy dispersive X-ray spectrum, the effect of ligating solvent on the formation of nanorods, and relaxivity curves. This material is available free of charge via the Internet at http://pubs.acs.org.